EPJ Web of Conferences **175**, 07036 (2018) https://doi.org/10.1051/epjconf/201817507036
Lattice 2017

Fluctuations of conserved charges from imaginary chemical potential

Jana N. Guenther[1,⋆], *Szabolcs* Borsányi[2], *Zoltan* Fodor[2,4,5], *Sandor D.* Katz[4], *Attila* Pásztor[2], and *Claudia* Ratti[3]

[1] *Department of Physics, University of Regensburg, Universitätsstraße 31, 93053 Regensburg, Germany*
[2] *Department of Physics, University of Wuppertal, Gaussstraße 20, 42119 Wuppertal, Germany*
[3] *Department of Physics, University of Houston, Houston, TX 77204, USA*
[4] *Institute for Theoretical Physics, Eötvös University, H-1117 Budapest, Hungary*
[5] *Jülich Supercomputing Centre, Forschungszentrum Jülich, 52425*

Abstract. When comparing lattice calculation to experimental data from heavy ion collision experiments, the higher order fluctuations of conserved charges are important observables. An efficient way to study these fluctuations is to determine them from simulations at imaginary chemical potential. In this talk we present results up to the six order derivative in μ_B (with up to eighth order included in the fit), calculated on a $48^3 \times 12$ lattice with staggered fermions using different values of μ_B while $\mu_S = \mu_Q = 0$.

1 Introduction

To analyse the quark gluon plasma that is created in heavy ion collision experiments at the LHC or RHIC a theoretical understanding of the deconfinement region of QCD is needed. Lattice QCD is a good tool to study QCD since this area can not be accessed perturbatively. At the moment direct simulations that are continuum extrapolated and at physical quark masses are restricted to vanishing or imaginary chemical potential. On the other hand the collisions especially at RHIC take place away from the axis of zero μ_B [1]. Therefore information in that region are needed. Even though it is not possible to do direct lattice simulations, it is possible to extrapolate observables from zero or imaginary chemical potential. This method is called analytical continuation. The analytical continuation from imaginary potential is by now well established (see for example [2–5]).

In this proceeding we present preliminary results on the fluctuations of conserved charges. These fluctuations can be measured on the particle distributions in heavy ion collisions (see for example [6]). A comparison between the experimental measurements and the theoretical calculations allows then for the determination of the order of the transition. A similar analysis form simulations at imaginary chemical potential was done in [5], that we will improve upon by presenting calculations to higher orders in μ_B. Results on the same observables were also studied by the Taylor expansion method and published in [7]. This method relies on simulations at $\mu_B = 0$ and calculates the analytical continuation from the measured derivatives.

⋆Speaker, e-mail: Jana.Guenther@t-online.de

All results shown in this proceeding are preliminary as the systematic error has not yet been properly determined. Especially the error from different higher order terms are not yet included. Further details on the error treatment for this analysis are given in section 3.4.

2 Lattice details

We use a tree-level Symanzik improved gauge action, with four times stout smeared ($\rho = 0.125$) staggered fermions. We simulate $2+1+1$ dynamical quarks where the light flavors are tuned in a way to reproduce the physical pion and kaon mass and we set $\frac{m_c}{m_s} = 11.85$ [8]. For the zero temperature runs we use large volumes which full fill $Lm_\pi > 4$. The scale is determined via f_π. More Details can be found in [9].

The maximal useful value of m_B is $m_B = i\pi T$ because of the Roberge-Weiss transition [10]. We simulate at eight different values of m_B given as: $\mu_B^{(j)} = iT\frac{j\pi}{8}$ for $j \in \{0, 1, 2, 3, 4, 5, 6, 7\}$. The analysis is done purely on a $48^3 \times 12$ lattice without continuum extrapolation, at twenty-two temperatures in the temperature range $140 \ldots 250$ MeV. All simulations are done at $\mu_Q = \mu_S = 0$. The ratios of the cumulates however are calculated at $\langle n_S \rangle = 0$ and $\langle n_Q \rangle = 0.4\langle n_B \rangle$ to match the conditions in heavy ion collisions.

3 Analysis

We present our analysis in three steps. We start with the analysis for $\chi_2^B, \chi_4^B, \chi_6^B$ and χ_8^B where we use the notation

$$\chi_{i,j,k}^{B,Q,S} = \frac{\partial^{i+j+k}(p/T^4)}{(\partial\hat{\mu}_B)^i(\partial\hat{\mu}_Q)^j(\partial\hat{\mu}_S)^k}, \tag{1}$$

with

$$\hat{\mu}_i = \frac{\mu_i}{T}. \tag{2}$$

First we do the analysis for each temperature separately (section 3.1). Afterwards we use the information that the results are expected to lie on a smooth curve, by introducing a spline through the results (section 3.2). Finally we use the same techniques introduced for χ_i^B to calculate three different ratios of the cumulants of the baryon distribution at $\langle n_S \rangle = 0$ and $\langle n_Q \rangle = 0.4\langle n_B \rangle$ in terms of the $\chi_{i,j,k}^{B,Q,S}$ (section 3.3).

3.1 Single Temperature

As a first step we analyse the data for a single temperature. For each $\mu_B \neq 0$ we measure $\chi_1^B, \chi_2^B, \chi_3^B$ and χ_4^B, while for $\mu_B = 0$ only χ_2^B and χ_4^B are measured since χ_1^B and χ_3^B are odd functions in μ_B and therefore equal to zero.

We make the ansatz for the partition sum:

$$\chi_0^B\hat{\mu}_B = c_0 + c_2\hat{\mu}_B^2 + c_4\hat{\mu}_B^4 + c_6\hat{\mu}_B^6 + c_8\hat{\mu}_B^8. \tag{3}$$

From this we can calculate the derivatives that we can measure on the lattice:

$$\chi_1^B\hat{\mu}_B = 2c_2\hat{\mu}_B + 4c_4\hat{\mu}_B^3 + 6c_6\hat{\mu}_B^5 + 8c_8\hat{\mu}_B^7 \tag{4}$$

$$\chi_2^B\hat{\mu}_B = 2c_2 + 12c_4\hat{\mu}_B^2 + 30c_6\hat{\mu}_B^4 + 56c_8\hat{\mu}_B^6 \tag{5}$$

$$\chi_3^B\hat{\mu}_B = 24c_4\hat{\mu}_B + 120c_6\hat{\mu}_B^3 + 336c_8\hat{\mu}_B^5 \tag{6}$$

$$\chi_4^B\hat{\mu}_B = 24c_4 + 360c_6\hat{\mu}_B^2 + 1680c_8\hat{\mu}_B^4. \tag{7}$$

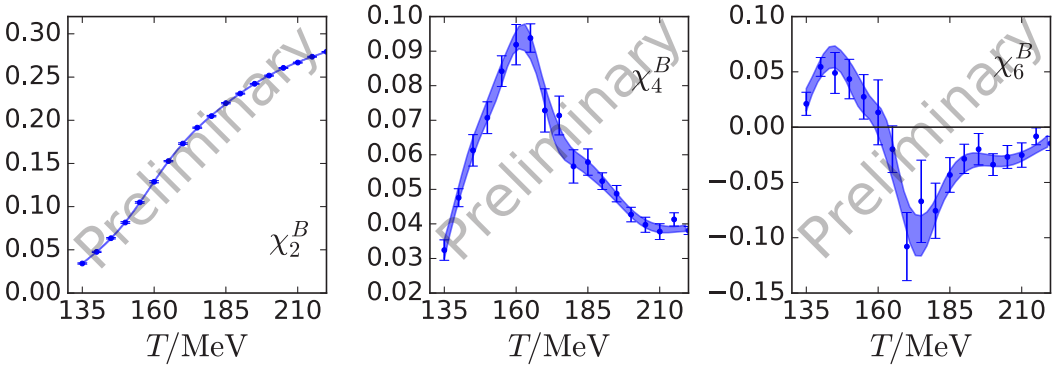

Figure 1. Preliminary results for χ_2^B, χ_4^B and χ_6^B

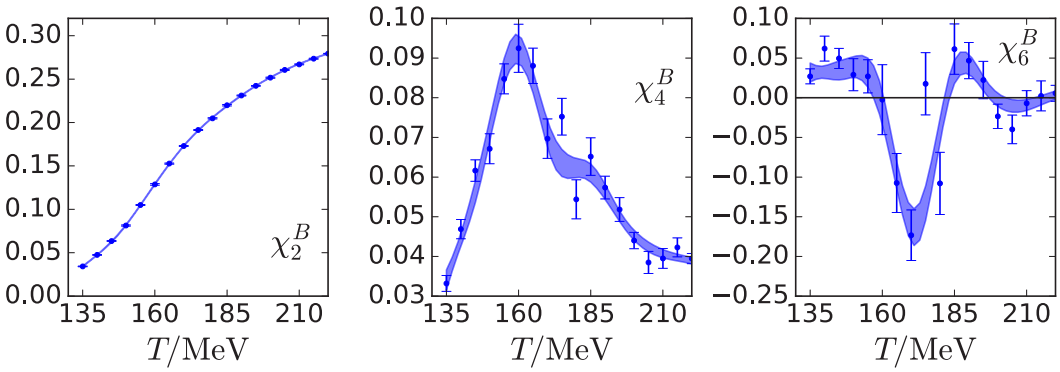

Figure 2. Preliminary results for χ_2^B, χ_4^B and χ_6^B when χ_8^B is included in the fit.

In a first step we determine the coefficients c_2, c_4 and c_6 from a correlated fit to the data, while c_8 is set to zero. The results are shown as blue points in figure 1. This ansatz does not account for the systematic uncertainties that arise from higher order contributions in $\frac{\mu_B}{T}$. As a first estimate for this uncertainties we include c_8 in our fit and check for changes in c_2 to c_6. The results are shown in figure 2. While the results for χ_2^B and χ_4^B are mostly unchanged, the changes for χ_6^B after the inclusion of χ_8^B are significant. Here it becomes obvious that a careful investigation of the influences of higher orders are necessary.

3.2 Spline Fit

We expect our results for $\chi_i^B(T)$ to lie on a smooth curve. We implement this information by fitting the results with a spline. Therefore the fit parameters c_2 , c_4, c_6 and c_8 now become functions of T themselves. For the spline fitting procedure the choice of note points is crucial. To reduce the bias that is implemented with a specific choice we have three different modes. The first and possibley simplest

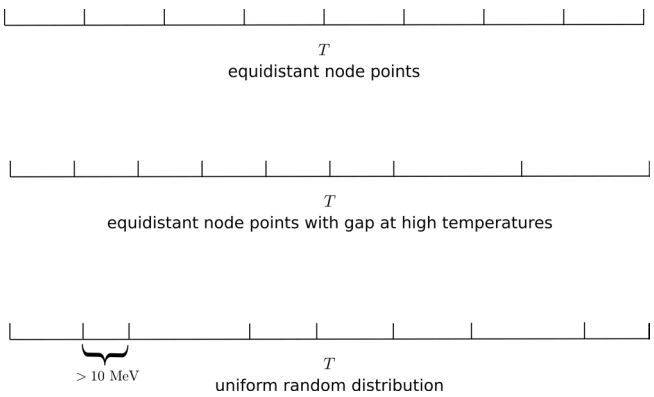

Figure 3. Different techniques for choosing the spline node points.

method is just to have all note points evenly spaced. However at higher temperatures we expect slower changes in our curves. Also for $\mu_B = 0$ our simulation points at high temperatures are more sparse. Therefore as a second choice we double the distance between the last three note points. As a last possibility we chose our note points randomly, with a uniform distribution. However to avoid the case of two note points that are very close to each other we only except a configuration if the distance between two neighbouring note points is at least 10 MeV. An illustration of this different node point configurations is shown in figure 3. Also the number of note points is varied between six and eight. The results are shown by the blue band in figure 1 and figure 2.

3.3 Cumulants

For a comparison with heavy ion collision experiments the cumulants of the net baryon distribution are a useful tool. The first four cumulants are the mean M_B, the variance σ_B^2, the skewness S_B and the kurtosis κ_B. By forming appropriate ratios, we can cancel out explicit volume factors. However the measured distributions themselves may still depend on the volume, which one should take into account, when comparing to experiments.

Heavy ion collisions with lead or gold take place with at $\mu_B > 0$, $\langle n_S \rangle = 0$ and $\langle n_Q \rangle = 0.4\langle n_B \rangle$. Since our simulations are done at $\mu_S = \mu_Q = 0$ and $\mu_B \neq 0$ we have to do some calculations to arrive at the same observables that are measured in experiments (see for example [6]). We investigate three different rations of cumulants and write each as a Taylor expansion:

$$\frac{M_B}{\sigma_B^2} = \frac{\chi_1^B(T,\hat{\mu}_B)}{\chi_2^B(T,\hat{\mu}_B)} = \hat{\mu}_B r_{12}^{B,1} + \hat{\mu}_B^3 r_{12}^{B,3} + \dots \tag{8}$$

$$\frac{S_B \sigma_B^3}{M_B} = \frac{\chi_3^B(T,\hat{\mu}_B)}{\chi_1^B(T,\hat{\mu}_B)} = r_{31}^{B,0} + \hat{\mu}_B^2 r_{31}^{B,2} + \dots \tag{9}$$

$$\kappa_B \sigma_B^2 = \frac{\chi_4^B(T,\hat{\mu}_B)}{\chi_2^B(T,\hat{\mu}_B)} = r_{42}^{B,0} + \hat{\mu}_B^2 r_{42}^{B,2} + \dots \tag{10}$$

The μ_B dependence of the $\chi_i^B(T, \hat{\mu}_B)$ can be again written in terms of the Taylor expansion:

$$\chi^{BQS}_{i,j,k}(\hat{\mu}_B) = \chi^{BQS}_{i,j,k}(0) + \hat{\mu}_B \left[\chi^{BQS}_{i+1,j,k}(0) + q_1\chi^{BQS}_{i,j+1,k}(0) + s_1\chi^{BQS}_{i,j,k+1}(0)\right] \tag{11}$$

$$+ \frac{1}{2}\hat{\mu}_B^2 \left[\chi^{BQS}_{i+2,j,k}(0) + s_1^2\chi^{BQS}_{i,j+2,k}(0) + q_1^2\chi^{BQS}_{i,j,k+2}(0)\right. \tag{12}$$

$$\left. +2q_1 s_1\chi^{BQS}_{i,j+1,k+1}(0) + 2s_1\chi^{BQS}_{i+1,j+1,k}(0) + 2q_1\chi^{BQS}_{i+1,j,k+1}(0)\right] + \ldots \tag{13}$$

$$\tag{14}$$

with

$$q_j = \frac{1}{j!}\frac{d^j\hat{\mu}_Q}{(d\hat{\mu}_B)^j}(0) \tag{15}$$

$$s_j = \frac{1}{j!}\frac{d^j\hat{\mu}_S}{(d\hat{\mu}_B)^j}(0) \tag{16}$$

We can now use the constrains $\langle n_S \rangle = 0$ and $\langle n_Q \rangle = 0.4\langle n_B \rangle$ which can be rewritten as

$$\chi_1^Q = 0.4\chi_1^B, \qquad \chi_1^S = 0 \tag{17}$$

to determine $r_{ij}^{B,k}$ coefficients form the equations 8, 9 and 10. However we now need to know not only the behaviour of the χ_i^B but also of derivatives with respect to μ_S and μ_Q. For now our simulations are restricted to ensembles with finite μ_B. Therefore the μ_S and μ_Q derivatives have to be calculated directly and without the support from the fit that we used in the μ_B direction. We calculate various $\chi^{B,Q,S}_{i,j,k}$ with the appropriate values of j and k and all possible values for i so that

$$i + j + k \leq 4. \tag{18}$$

For each group of fluctuations with the same j and k we perform a fit analogous to the procedure described in the sections 3.1 and 3.2. This is sufficient to determine the first to $r_{ij}^{B,k}$ coefficients for all three observables. The results are shown in figure 4, 5 and 6. For higher order coefficients, higher order derivatives in μ_S and μ_Q are needed. The direct measurements have a rapidly increasing error with each derivative and very large statistics would be needed to improve our calculations in that manner. Another possibility would be add ensembles with finite μ_S and μ_Q and do a similar fit as for the μ_B direction. This approach has been used in [5].

3.4 Error Analysis

For a reliable comparison between experimental measurements and theoretical calculations the error estimation is an important ingredient. As we present work in progress results the error estimation process is not yet finished. Our statistical error is estimated by the Jack-Knife-Method. For our systematic error there are several sources, which we have not yet completely covered. We determine our systematic error by the histogram method described in [11], where each analysis is weighted with the akaike information criteria. We include the influence of the number of points in the μ_B direction, by either including or ignoring the data from our highest value for μ_B. We also try to estimate the influence of the spline node points as described in section 3.2. However a very important source for our systematic error is the influence of the higher order contributions in μ_B that are not included in our fit ansatz. A rough idea of this influences can be gained from the comparison of the results shown in figure 1 and figure 2, where one order more was included. However a more detailed analysis is necessary to obtain a reliable error on our result.

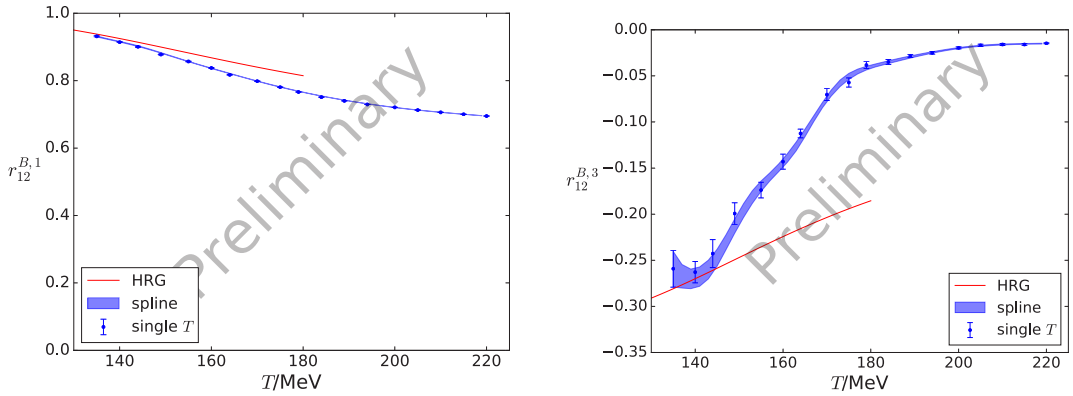

Figure 4. $\frac{M_B}{\sigma_B^2} = \frac{\chi_1^B(T,\hat{\mu}_B)}{\chi_2^B(T,\hat{\mu}_B)} = \hat{\mu}_B r_{12}^{B,1} + \hat{\mu}_B^3 r_{12}^{B,3} + \ldots$

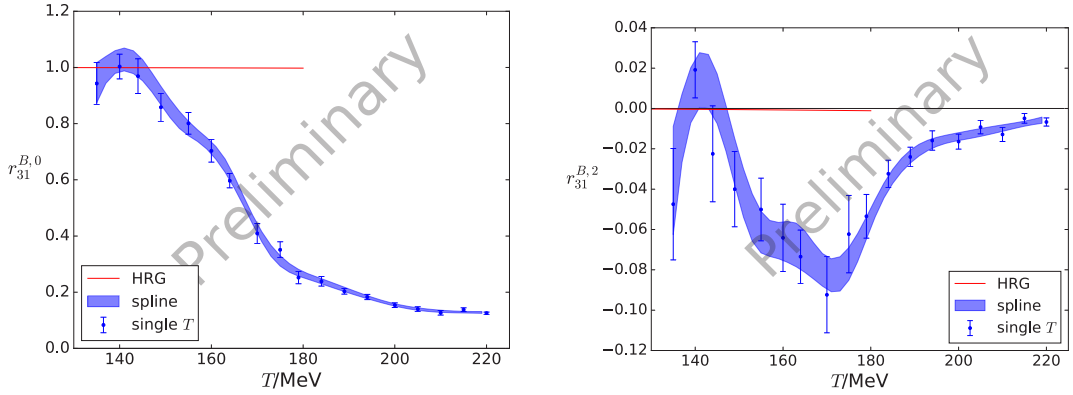

Figure 5. $\frac{S_B\sigma_B^3}{M_B} = \frac{\chi_3^B(T,\hat{\mu}_B)}{\chi_1^B(T,\hat{\mu}_B)} = r_{31}^{B,0} + \hat{\mu}_B^2 r_{31}^{B,2} + \ldots$

4 Conclusion

We presented preliminary results on fluctuations of conserved charges χ_2^B, χ_4^B and χ_6^B and on the three combinations of cumulants $\frac{M_B}{\sigma_B^2}$, $\frac{S_B\sigma_B^3}{M_B}$ and $\kappa_B\sigma_B^2$ that can be measured by havy ion collision experiments. We calculated the Taylor expansion of each of these three observables to NLO in μ_B. Our analysis was done on an $48^3 \times 12$ lattice. To match experimental conditions $\frac{M_B}{\sigma_B^2}$, $\frac{S_B\sigma_B^3}{M_B}$ and $\kappa_B\sigma_B^2$ have been calculated at the strangeness neutral point $\langle n_S \rangle = 0$ and with $\langle n_Q \rangle = 0.4\langle n_B \rangle$. The error investigation is for now mostly limited to the statistical error. Especially an investigation of the influence of higher order continuations is necessary to arrive at a final result.

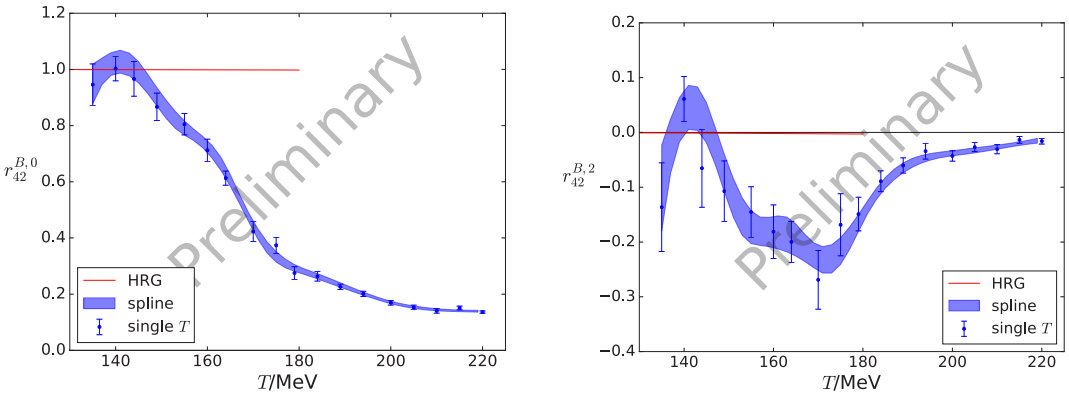

Figure 6. $\kappa_B\sigma_B^2 = \frac{\chi_4^B(T,\hat{\mu}_B)}{\chi_2^B(T,\hat{\mu}_B)} = r_{42}^{B,0} + \hat{\mu}_B^2 r_{42}^{B,2} + \ldots$

Acknowledgement

This project was funded by the DFG grant SFB/TR55. This material is based upon work supported by the National Science Foundation through grant number NSF PHY-1654219 and by the U.S. Department of Energy, Office of Science, Office of Nuclear Physics, within the framework of the Beam Energy Scan Theory (BEST) Topical Collaboration. An award of computer time was provided by the INCITE program. This research used resources of the Argonne Leadership Computing Facility, which is a DOE Office of Science User Facility supported under Contract DE-AC02-06CH11357. The authors gratefully acknowledge the Gauss Centre for Supercomputing (GCS) for providing computing time for a GCS Large-Scale Project on the GCS share of the supercomputer JUQUEEN [13] at Julich Supercomputing Centre (JSC). The authors gratefully acknowledge the use of the Maxwell Cluster and the advanced support from the Center of Advanced Computing and Data Systems at the University of Houston.

References

[1] G. Odyniec, EPJ Web Conf. **95**, 03027 (2015)
[2] P. de Forcrand, O. Philipsen, Nucl. Phys. **B642**, 290 (2002), hep-lat/0205016
[3] C. Bonati, M. D'Elia, M. Mariti, M. Mesiti, F. Negro, F. Sanfilippo, Phys. Rev. **D92**, 054503 (2015), 1507.03571
[4] P. Cea, L. Cosmai, A. Papa, Phys. Rev. **D93**, 014507 (2016), 1508.07599
[5] M. D'Elia, G. Gagliardi, F. Sanfilippo, Phys. Rev. **D95**, 094503 (2017), 1611.08285
[6] L. Adamczyk et al. (STAR), Phys. Rev. Lett. **112**, 032302 (2014), 1309.5681
[7] A. Bazavov et al., Phys. Rev. **D95**, 054504 (2017), 1701.04325
[8] C. McNeile, C.T.H. Davies, E. Follana, K. Hornbostel, G.P. Lepage, Phys. Rev. **D82**, 034512 (2010), 1004.4285
[9] R. Bellwied, S. Borsanyi, Z. Fodor, J. Günther, S.D. Katz, C. Ratti, K.K. Szabo, Phys. Lett. **B751**, 559 (2015), 1507.07510
[10] A. Roberge, N. Weiss, Nucl. Phys. **B275**, 734 (1986)
[11] S. Durr et al., Science **322**, 1224 (2008), 0906.3599
[12] Jülich Supercomputing Centre, Journal of large-scale research facilities **A1**, 1 (2015)